

Impact of the [C II]_{158μm} luminosity scatter on the line-intensity mapping power spectrum from the EoR

Chandra Shekhar Murmu^{1*}, Karen P. Olsen², Thomas R. Greve^{3,4,5}, Suman Majumdar^{1,6}, Kanan K. Datta⁷, Bryan R. Scott⁸, T. K. Daisy Leung⁹, Romeel Dave^{10,11,12}, Gergö Popping¹³, Raul Ortega Ochoa^{3,4}, David Vizgan^{3,4,14,15}, and Desika Narayanan^{16,17,3}

¹Department of Astronomy, Astrophysics and Space Engineering, Indian Institute of Technology Indore, Khandwa Rd., Simrol 453552, India

²Department of Astronomy and Steward Observatory, University of Arizona, Tucson, AZ 85721, USA

³Cosmic Dawn Center (DAWN)

⁴National Space Institute, DTU Space, Technical University of Denmark, Elektrovej 327, DK-2800 Kgs. Lyngby, Denmark

⁵Department of Physics and Astronomy, University College London, Gower Street, London WC1E 6BT, UK

⁶Department of Physics, Blackett Laboratory, Imperial College, London SW7 2AZ, UK

⁷Department of Physics, Presidency University, 86/1 College St., Kolkata 700073, India

⁸Department of Physics & Astronomy, University of California, Riverside, USA

⁹Center for Computational Astrophysics, Flatiron Institute, 162 Fifth Avenue, New York, NY 10010, USA

¹⁰Institute for Astronomy, Royal Observatory, University of Edinburgh, Edinburgh EH9 3HJ, UK

¹¹University of the Western Cape, Bellville, Cape Town 7535, South Africa

¹²South African Astronomical Observatories, Observatory, Cape Town 7925, South Africa

¹³European Southern Observatory, Karl-Schwarzschild-Straße, D-85748 Garching, Germany

¹⁴Astronomy Department and Van Vleck Observatory, Wesleyan University, 96 Foss Hill Drive, Middletown, CT 06459, USA

¹⁵Department of Astronomy, University of Illinois at Urbana-Champaign, 1002 West Green St., Urbana, IL 61801, USA

¹⁶Department of Astronomy, University of Florida, 211 Bryant Space Sciences Center, Gainesville, FL 32611, USA

¹⁷University of Florida Informatics Institute, 432 Newell Drive, CISE Bldg. E251, Gainesville, FL 32611, USA

Accepted XXX. Received YYY; in original form ZZZ

ABSTRACT

Redshifted [C II]_{158μm} line-intensity mapping (LIM) of the Epoch of Reionization (EoR) with ongoing and upcoming experiments like the CONCERTO, TIME and FYST, is a new tool to constrain the role of the early galaxies in reionization. We expect statistics, e.g., the power spectrum of the LIM signal to be detectable by these experiments, which will help us understand the large-scale distribution and astrophysical properties of the [C II]_{158μm} line emitters. In this work, unlike a simple semi-analytical approach, we derive the [C II]_{158μm} line-luminosity scatter, which arises from various ongoing astrophysical processes under varied environments inside individual galaxies, from a hydrodynamic and radiative transfer simulation of galaxies, to interpret its impact on the power spectrum. We compare the luminosity scatter scenario with best-fit relations obtained from mean and most probable $L_{[\text{CII}]}$ values and find that in both cases, along with a slight, unavoidable diminishing of the luminosity-weighted halo bias, the clustering (large-scale) power spectrum is impacted significantly, in addition to the shot-noise component. In the latter case, the power spectrum is enhanced by a factor of $\sim 2.7 - 2.9$ for $0.1 \leq k \leq 1 \text{ Mpc}^{-1}$ (at $z = 6$); we present this alternative approach to interpret this enhancement in the clustering power in conjunction with a simple analytical model. It is crucial to appropriately model and take line-luminosity scatter into account to interpret the [C II]_{158μm} power spectrum from future observations.

Key words: cosmology: large-scale structure of Universe – galaxies: haloes, high-redshift – methods: numerical, statistical, analytical

1 INTRODUCTION

Probing the early galaxies from the Epoch of Reionization (EoR) is challenging, demanding very high resolution and sensitivities from the instruments trying to probe these galaxies. Observatories like HST (Robertson et al. 2015), ALMA (Fèvre et al. 2020) and upcoming instruments like JWST, can detect these galaxies in small

numbers. However, point-source detections through spectroscopy or photometry are expensive because they consume a significant amount of observational time.

Line-intensity mapping (LIM) of galaxies (Visbal & Loeb 2010; Gong et al. 2011a) is a possible solution for this, by which one can detect the integrated flux of atomic or molecular line emissions from numerous sources at once, without resolving them individually and with reduced sensitivity requirements. Moreover, it will significantly cut down the observational hours required to map large volumes of

* E-mail: chandra0murmu@gmail.com (CSM)

the sky and probe numerous samples, to infer about the statistical properties of the source distribution. The $[\text{C II}]_{158\mu\text{m}}$ emission line is a promising candidate for LIM (Gong et al. 2011b; Silva et al. 2015; Dumitru et al. 2019; Yue & Ferrara 2019; Sun et al. 2021; Murmu et al. 2021), and experiments like CONCERTO (Lagache 2017; The CONCERTO Collaboration et al. 2020), TIME (Crities et al. 2014; Sun et al. 2021), FYST (Cothard et al. 2020; CCAT-Prime collaboration et al. 2021), TIM (Vieira et al. 2020) are already targeting this line to detect the early galaxies with LIM.

These LIM experiments will be capturing the sky-fluctuations of the $[\text{C II}]_{158\mu\text{m}}$ line emission, enabling us to estimate valuable statistics like the power spectrum of the signal. Using the signal power spectrum, we will understand the large-scale distribution and astrophysical properties of these ionizing sources from the EoR. Previous studies (Li et al. 2016; Schaan & White 2021; Yang et al. 2021) have shown the line emission scatter to enhance the shot-noise power spectrum of the LIM signal. Here, unlike a simple semi-analytical approach, we derive the luminosity scatter of $[\text{C II}]_{158\mu\text{m}}$ emission from a hydrodynamic and radiative transfer simulation of galaxies. We try to interpret the impact of scatter on the power spectrum by comparing the $[\text{C II}]_{158\mu\text{m}}$ LIM map developed from best-fit $L_{[\text{C II}]}-M_{\text{halo}}$ relation, obtained from the mean $L_{[\text{C II}]}$ and most probable $L_{[\text{C II}]}$ values of $L_{[\text{C II}]}$ distribution, with the $[\text{C II}]_{158\mu\text{m}}$ LIM map with scatter. We find that in both cases, along with a slight diminishing in the luminosity-weighted halo bias, the clustering (large-scale) power spectrum is enhanced significantly compared to the best fit, in addition to the shot-noise component. Interestingly, a recent study by Moradinezhad Dizgah et al. (2021) also supports our finding that the clustering power spectrum might be significantly boosted under line luminosity scatter. As shown in Leung et al. (2020), which employed the cosmological hydrodynamics simulation SIMBA (Davé et al. 2019; Leung et al. 2020; Hassan et al. 2021) coupled with CLOUDY (Ferland et al. 2013, 2017) and sFAME (Olsen et al. 2015, 2016, 2017; Leung et al. 2020) to model the $[\text{C II}]_{158\mu\text{m}}$ line emission from a large number of simulated galaxies, we expect a significant scatter in the $L_{[\text{C II}]}$ versus M_{halo} relationship, which is of astrophysical origin. We have remapped the scatter predicted by Leung et al. (2020) on the halo distribution obtained from a large volume N-body simulation to interpret the impact of this $[\text{C II}]_{158\mu\text{m}}$ luminosity scatter on the observed LIM power spectrum.

We have organised this paper into the following sections: First, we discuss the scatter in the $[\text{C II}]_{158\mu\text{m}}$ luminosity in section 2. Next, the methods of simulating the $[\text{C II}]_{158\mu\text{m}}$ LIM signal and estimating the power spectrum are described in section 3. We then discuss our results in section 4 and finally summarize the paper in section 5. Throughout this work, we have adopted cosmological parameters $\Omega_m = 0.3183$, $\Omega_\Lambda = 0.6817$, $h = 0.6704$, $\Omega_b h^2 = 0.022032$, $\sigma_8 = 0.8347$, $n_s = 0.9619$, consistent with Planck+WP best-fit values (Planck Collaboration et al. 2014).

2 $[\text{C II}]_{158\mu\text{m}}$ LUMINOSITY SCATTER

The $[\text{C II}]_{158\mu\text{m}}$ luminosity scatter originates from the collective dependence of $L_{[\text{C II}]}$ on various astrophysical factors such as star formation, metal enrichment, and different phases of the interstellar medium (ISM). The sFAME simulations by Leung et al. (2020) handle three ISM phases (ionized, atomic, and molecular) all of which emit $[\text{C II}]_{158\mu\text{m}}$. The molecular phase, which makes up no more than ~ 30 per cent of the total ISM mass in the simulations, typically contributes by more than 50 per cent to the total $[\text{C II}]_{158\mu\text{m}}$ emission, especially in massive galaxies ($M_\star > 10^9 M_\odot$). The con-

tribution to the $[\text{C II}]_{158\mu\text{m}}$ emission from the ionized and atomic gas can be up to 50 per cent but decreases with increasing stellar mass and metallicity. Although one would expect the $[\text{C II}]_{158\mu\text{m}}$ emission to decrease at lower metallicities, this effect is negligible compared to the increase in CO photo-dissociation rate (and thus the available C^+ ions) that comes with lower metallicities. The scatter in the $L_{[\text{C II}]}$ versus M_{halo} relation, therefore, primarily comes from the scatter in the relative mass distributions of the ISM phases, which in turn is set by the specific star-formation rate and metallicity. Although $L_{[\text{C II}]}$ is correlated to the host halo-mass, we would expect that, in reality, it doesn't follow a one-to-one dependence. In the following subsections, we discuss the method of simulating the $[\text{C II}]_{158\mu\text{m}}$ emission from galaxies and obtaining a one-to-one $L_{[\text{C II}]}$ versus M_{halo} fit to the $L_{[\text{C II}]}$ scatter.

2.1 Simulations of $[\text{C II}]_{158\mu\text{m}}$ emission

This work builds on the analysis of snapshots taken from the SIMBA suite of cosmological galaxy formation simulations, which themselves were evolved using the meshless finite mass hydrodynamics technique of GIZMO (Hopkins 2015, 2017; Davé et al. 2019). The SIMBA simulation set consists of three cubical volumes, each of 25, 50 and $100 h^{-1} \text{ cMpc}$ ($h = 0.678$) on each sides, all of which are used in this work to search for galaxies at $z \sim 6$. For each volume, a total of 1024^3 gas elements and 1024^3 dark matter particles are evolved from $z = 249$. The galaxy properties in SIMBA have been compared to various observations across cosmic time (Thomas et al. 2019; Appleby et al. 2020), including the epoch of reionization (Wu et al. 2020; Leung et al. 2020), and are in reasonable agreement. The sample of galaxies used here is the same as that presented in Leung et al. (2020) and consists of 11,125 galaxies, with derived $[\text{C II}]_{158\mu\text{m}}$ luminosities from $10^{3.82}$ to $10^{8.91} L_\odot$.

In order to derive the $[\text{C II}]_{158\mu\text{m}}$ emission, the galaxy samples were post-processed with version 2 of the sFAME module (Olsen et al. 2017).¹ This version of sFAME uses the spectral synthesis code CLOUDY (v17.01; Ferland et al. 2013, 2017), to model the line emission from the multi-phased ISM within each simulated galaxy. As input to CLOUDY, sFAME uses physically motivated prescriptions to calculate the local interstellar radiation field (ISRF) spectrum, the cosmic ray (CR) ionization rate, and the gas density distribution of the ionized, atomic and molecular ISM phases (see Davé et al. (2019) and Leung et al. (2020) for details on the SIMBA simulation and implementation of sFAME, respectively).

2.2 Fitting the $[\text{C II}]_{158\mu\text{m}}$ luminosity scatter

We derive the halo $[\text{C II}]_{158\mu\text{m}}$ luminosity from the central galaxies' $[\text{C II}]_{158\mu\text{m}}$ luminosity; these central galaxies are identified in the SIMBA simulation. We fit the $[\text{C II}]_{158\mu\text{m}}$ luminosity scatter with a one-to-one $L_{[\text{C II}]}-M_{\text{halo}}$ model; this fit is used to interpret the impact of $[\text{C II}]_{158\mu\text{m}}$ luminosity scatter on the power spectrum. The data from SIMBA simulation were used to obtain the fit.

We have used the scaling relation from Leung et al. (2020), where the one-to-one $L_{[\text{C II}]}-M_{\text{halo}}$ relationship is given by

$$\log\left(\frac{L_{[\text{C II}]}}{L_\odot}\right) = C + a \log\left(\frac{M_h}{M_a}\right) + b \log\left(1 + \frac{M_h}{M_b}\right). \quad (1)$$

The scatter can be fitted using multiple approaches. In Leung et al.

¹ <https://kpolsen.github.io/SFAME/index.html>

(2020), the fit is to the arithmetic mean of L_{CII} , whereas here we have chosen to fit with the most probable values or modes of the $\log L_{\text{CII}}$ distributions. The $L_{\text{CII}}-M_{\text{halo}}$ scatter data were first binned with respect to the halo mass, and within each halo mass bin, the mode is picked up as the representative of the $\log L_{\text{CII}}$ distribution in that bin. We use them in a non-linear least-square fitting to estimate the best-fit values of the parameters for the one-to-one $L_{\text{CII}}-M_{\text{halo}}$ model. The parameter values were determined to be $a = 0.99$, $b = -9.85$, $C = 3.02$, $M_a = 6.2 \times 10^6 M_\odot$ and $M_b = 2.9 \times 10^{13} M_\odot$, corresponding to the black curve in fig. 1.

From the standpoint of galactic astrophysics, the line-luminosity scatter originates from the detailed astrophysical environments within and around the galaxies, as discussed in sec. 2. If we consider the population distribution of these galaxies relative to their $[\text{C II}]_{158\mu\text{m}}$ luminosity, we can use the peak of the distribution or the most probable values of L_{CII} to represent the corresponding halo mass bin. Therefore, this approach, although not precisely, conforms to a Bayesian fitting method. It is a robust alternative to interpret the impact of $[\text{C II}]_{158\mu\text{m}}$ luminosity scatter on the power spectrum.

The fit from Leung et al. (2020) is also shown in fig. 1 (dashed-magenta), and the parameters that differ in this case are $a = 0.97$, $C = 3.62$ and $M_a = 1.5 \times 10^7 M_\odot$. This fit was obtained by taking the arithmetic mean of L_{CII} over halo mass bins and then applying a non-linear least-square fit, and has a mean difference of 0.14 dex compared to the fit in this work. The following section describes the methods we used to estimate the $[\text{C II}]_{158\mu\text{m}}$ LIM power spectrum, which takes the $[\text{C II}]_{158\mu\text{m}}$ luminosity scatter into account. We interpret the impact of this scatter relative to both the scatter fitting methods discussed above.

3 [C II] 158 μm LIM POWER SPECTRUM WITH SCATTER

The simulation volumes in Leung et al. (2020) are not large enough to estimate the $[\text{C II}]_{158\mu\text{m}}$ power spectrum with good statistical significance. Furthermore, the number of galaxies in individual volumes is not high enough as well. To deal with these problems, we remapped the scatter generated in the simulation suite of Leung et al. (2020) in an N-body (Bharadwaj & Srikant 2004) dark matter-only simulation with a volume of 215^3 Mpc^3 . The collapsed halos in the N-body simulation were identified with an FoF (Mondal et al. 2015) algorithm, with a halo mass resolution of $\approx 10^9 M_\odot$.

The range of halo mass in both the simulations are similar, which eased this exercise of reproducing the scatter. First, we divide the halo mass range in into 20 log-arithmetic bins. Then, within each halo mass bin, we estimate the distribution of $[\text{C II}]_{158\mu\text{m}}$ luminosity from the original scatter. The next step is to generate values of $[\text{C II}]_{158\mu\text{m}}$ luminosity following the same distribution as the original one, within each halo mass bin. One way of doing that could be to generate random L_{CII} values using *inverse transform sampling*, in which values are sampled from the empirical cumulative distribution function (Vanderplas et al. 2012; Ivezić et al. 2014). However, here we modeled the original distribution from SIMBA with a *piecewise constant distribution*. Given the information about the $\log L_{\text{CII}}$ histogram, such as boundaries of the bin intervals and the probability densities, within each halo mass bin, we generate a random $\log L_{\text{CII}}$ value according to a probability density function given by

$$P(\log L_{\text{CII}} | l_0, \dots, l_n, w_0, \dots, w_{n-1}) = \frac{w_i}{\sum_{k=0}^{n-1} w_k (l_{k+1} - l_k)}. \quad (2)$$

Here $n + 1$ is the number of boundaries separating the intervals. l_i

are the boundaries of the intervals, with $0 \leq i \leq n$, and w_i are the corresponding weights or the probability densities, with $0 \leq i < n$. For a given L_{CII} , it will satisfy $l_i \leq \log L_{\text{CII}} < l_{i+1}$, with $0 \leq i < n$. Thus, within a certain bin, uniform $\log L_{\text{CII}}$ values are generated with a certain associated weight, such that the overall distribution is reproduced in an almost exact fashion. This implementation is quite simple enough and is adopted here from the C++ standard library.

Using this, we reproduced the actual scatter distribution present in the original simulation by Leung et al. (2020), in our N-body simulation. We also generated 1000 different realizations of such scatter distributions, and eventually that many number of $[\text{C II}]_{158\mu\text{m}}$ intensity maps were also developed. Finally, the power spectra were computed for each of these intensity maps and averaged over, for the case with L_{CII} scatter. The spatial distribution of the $[\text{C II}]_{158\mu\text{m}}$ line emitters in our simulation volume is directly sampled to estimate the power spectrum.

In fig. 2, we present snapshots of $[\text{C II}]_{158\mu\text{m}}$ maps for different scenarios, with and without L_{CII} scatter. The $[\text{C II}]_{158\mu\text{m}}$ maps from the leftmost and middle panel were developed using the fit from eq. 1 (as in Murmu et al. 2021), with the leftmost map using parametrization from the most probable L_{CII} values and the middle panel from Leung et al. (2020). The rightmost panel shows one of the $[\text{C II}]_{158\mu\text{m}}$ maps from many realizations with luminosity scatter. From visual inspection, the rightmost panel is overall brighter and has stronger intensity fluctuations relative to the leftmost panel. The histograms of the reproduced scatter are shown in green in the bottom panels of fig. 3, corresponding to the method of eq. 2. We can see subtle differences between the original histogram (top panels of fig. 3) and the reproduced one, although they are mostly similar.

We also reproduced the scatter using a cheaper alternative, by assuming that L_{CII} follows a log-normal distribution. First, for each halo mass bin, the mean and the standard deviation of $\log L_{\text{CII}}$ distribution are computed from the SIMBA data. Then, using these, we sample L_{CII} from a log-normal distribution for each halo mass bin and implement it on the N-body halos. In the bottom panels of fig. 3, the black-colored histogram corresponds to the log-normal approximation of the L_{CII} scatter. In the next section, we discuss the interpretation of the impact of luminosity scatter on the mean intensity and power spectrum.

4 RESULTS

4.1 Intensity of the [C II] 158 μm LIM signal

We find that the $[\text{C II}]_{158\mu\text{m}}$ maps, which we reproduced with scatter derived from the SIMBA simulation, have a mean intensity of $\sim 5.3 \times 10^2 \text{ Jy/sr}$. The map without any scatter, obtained from the fitting function using most probable L_{CII} values, has a mean intensity of $\sim 2.9 \times 10^2 \text{ Jy/sr}$, and therefore, the increment is by a factor of ~ 1.8 in this case. Now, for a given halo mass bin, the average luminosity with log-normal scatter is

$$\bar{L} = \int_{-\infty}^{\infty} d(\log L) L \times \frac{1}{\sqrt{2\pi}\sigma} \exp - \frac{(\log L - \log \hat{L})^2}{2\sigma^2}, \quad (3)$$

which we can rewrite as

$$\frac{\bar{L}(\sigma)}{\bar{L}_{\sigma=0}} = \int_{-\infty}^{\infty} dx \frac{10^{x\sqrt{2}\sigma}}{\sqrt{\pi}} \exp -x^2 \quad (4)$$

(see Moradinezhad Dizgah et al. 2021), with $\bar{L}_{\sigma=0} = \hat{L}$ being the average of L for $\sigma = 0$ (no scatter), and \hat{L} is the average of L in log-space. We find that the average σ for the halo mass bins considered

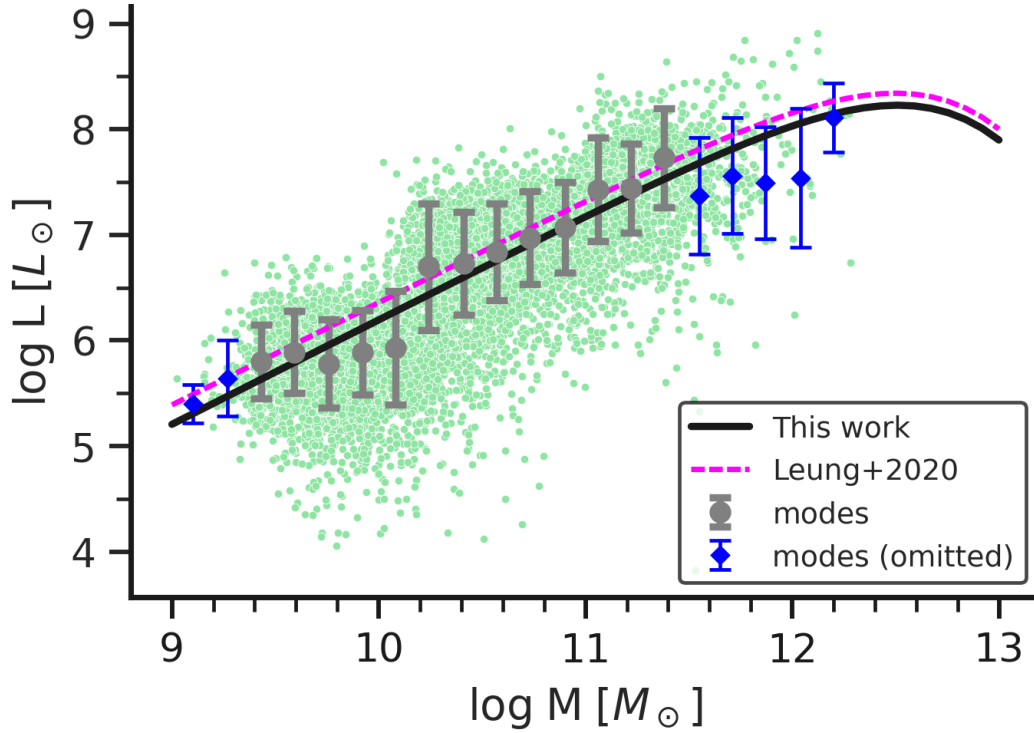


Figure 1. L_{CII} vs. M_{halo} scatter from SIMBA simulation is shown here in *green* dots, for $z = 6$. The points with error bars are the most probable values or *modes* of the L_{CII} distribution in each halo mass bin. The fit obtained in this work is shown in *black*-colored curve, with *blue*-points excluded in the fit due to poor sample numbers.

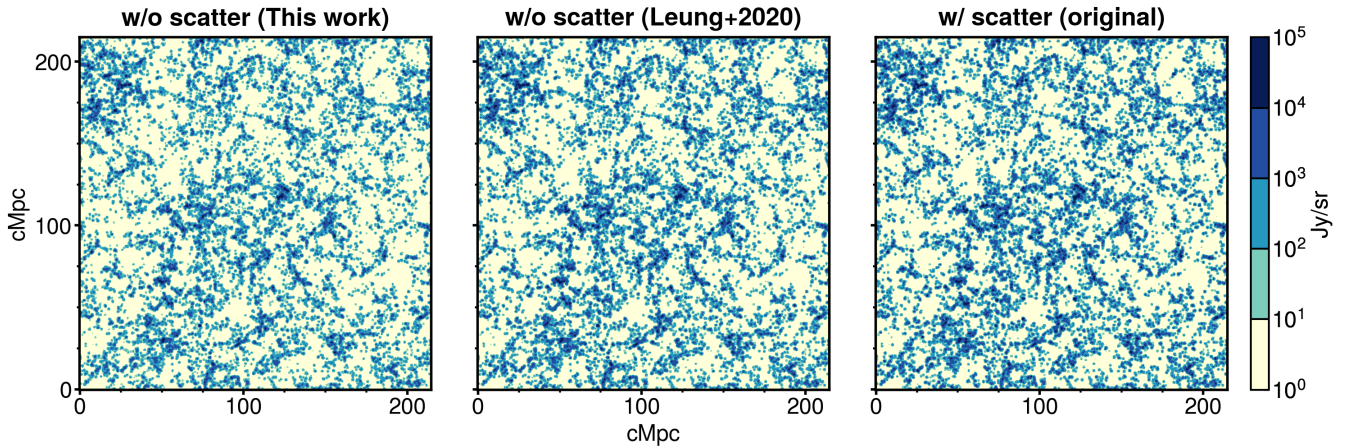


Figure 2. The $[\text{C II}]_{158\mu\text{m}}$ maps in left-most and middle panel are developed using eq. 1, without scatter, from N-body simulation. The right-most panel shows $[\text{C II}]_{158\mu\text{m}}$ map, with scatter implemented using the exact method.

in the fitting, from the SIMBA + SÍGAME results, is 0.45 dex which, when put in eq. 4, yields an approximate factor of enhancement in the mean intensity of ~ 1.7 , in agreement with our simulation result to 5 per cent. Therefore, using this simple model, we can interpret the mean intensity of the $[\text{C II}]_{158\mu\text{m}}$ maps with log-normal luminosity scatter.

In the other case, we use Leung et al. (2020) fit to generate $[\text{C II}]_{158\mu\text{m}}$ map and find that this results in mean intensity of $\sim 4.3 \times 10^2$ Jy/sr. When we interpret the mean intensity of the

$[\text{C II}]_{158\mu\text{m}}$ map including line-luminosity scatter, with this fit, we see an increment of ~ 23 per cent. Although Leung et al. (2020) fit uses the arithmetic mean of L_{CII} scatter from halo mass bins, it doesn't guarantee that the mean intensity of the $[\text{C II}]_{158\mu\text{m}}$ emission map will remain precisely invariant (as we see here) when the luminosity scatter is considered. We might expect this because the scatter is derived from the output of a realistic hydrodynamic and radiative-transfer simulation of galaxies, such that within each halo mass bin, the mean L_{CII} values will fluctuate. When we try to fit these values

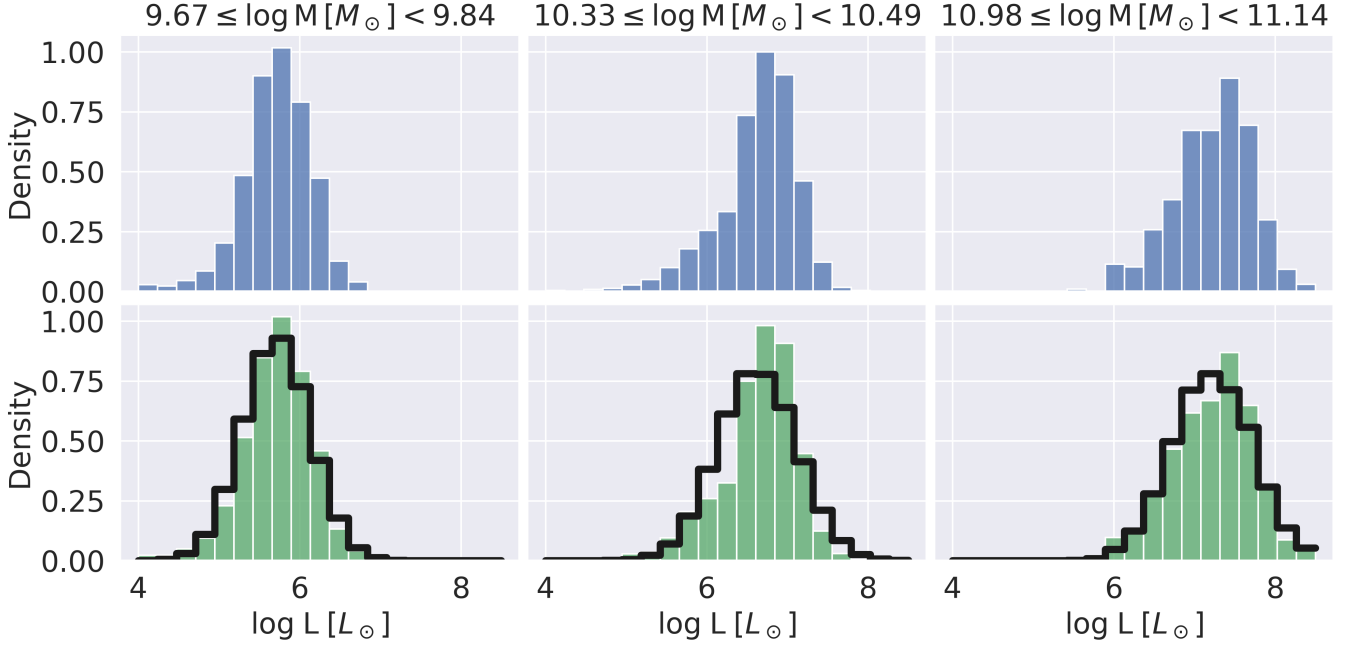


Figure 3. *Top:* L_{CII} distribution from SIMBA *Bottom:* L_{CII} distribution reproduced in N-body simulation from SIMBA data is shown. The *black-colored* histogram is the scatter reproduced from log-normal distribution.

with a smooth $L_{\text{CII}}-M_{\text{halo}}$ function, it doesn't pass through every such point (see Leung et al. 2020, fig. 6), and therefore we cannot expect this fit to keep the mean intensity invariant. However, whether we can model this change robustly is yet unclear and might require further analysis. Therefore, as is evident from this discussion, the change in the mean intensity is not an intrinsic phenomenon but depends on how we interpret the scatter relation between L_{CII} and M_{halo} . In the scenario of fluctuating mean L_{CII} values, one can always assume a one-to-one fit to exist, such that the mean intensity is the same as that of the $[\text{C II}]_{158\mu\text{m}}$ map with luminosity scatter. However, unlike the other two occasions discussed above, where we can parametrize the fit with a simple least-square or any other fitting method, obtaining this fit might not be straightforward and practical.

4.2 $[\text{C II}]_{158\mu\text{m}}$ power spectrum

We now come to the results of interpreting the $[\text{C II}]_{158\mu\text{m}}$ power spectrum with luminosity scatter relative to the no-scatter case. In fig. 4, we see an enhancement in the power spectrum by a factor of ~ 2.9 across $0.1 \leq k \leq 1 \text{ Mpc}^{-1}$ when compared to the fit obtained from most probable L_{CII} values. This enhancement is almost constant across the k -range considered, with no appreciable change in the slope. When we interpret the clustering and shot-noise components in this case, they do not have any relative dominance over each other. The increase in the clustering component is expected since we interpret the mean intensity to increase in this scenario. When we compare to the Leung et al. (2020) fit, the increment is > 30 per cent, with no change in slope and an increment in the clustering component (large-scale power spectrum).

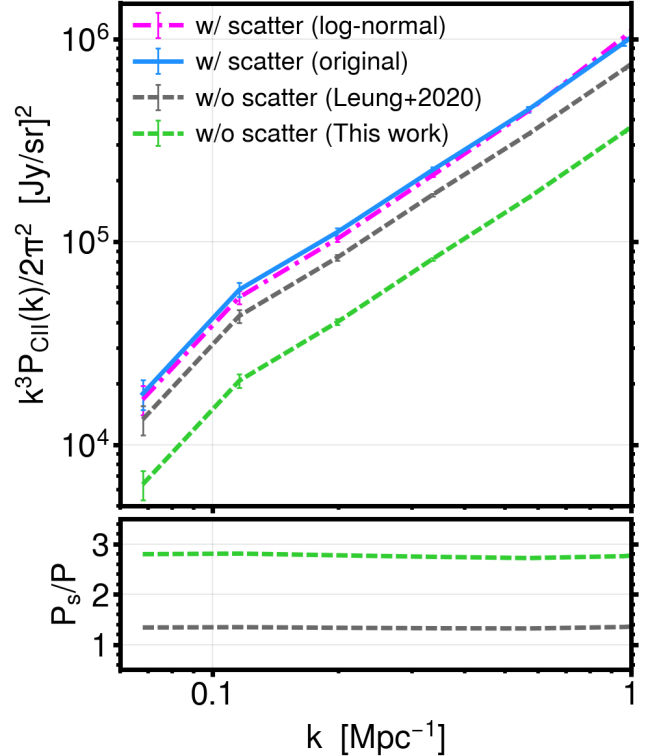


Figure 4. *Top:* $[\text{C II}]_{158\mu\text{m}}$ power spectrum at $z = 6$ with and without L_{CII} scatter *Bottom:* Dashed green represents ratio of power spectrum between scatter and fit with most probable L_{CII} values. Dashed grey represents ratio corresponding to scatter and fit with arithmetic mean of L_{CII} values.

4.3 Luminosity-weighted halo bias

Since the clustering power spectrum goes as $P_{[\text{CII}]}^{\text{clus}}(k, z) \propto \bar{L}_{[\text{CII}]}^2(z) \bar{b}_{[\text{CII}]}^2(z)$, we could have expected an enhancement of at least $\sim 1.8^2$ in the small k -modes but got only a maximum of 2.9 factor of increment compared to the fit obtained from most probable $L_{[\text{CII}]}$ values. We argue that the luminosity-weighted halo bias, given as

$$\bar{b}_{[\text{CII}]}(z) = \frac{\int dM \frac{dn}{dM} L_{[\text{CII}]}(M, z) b(M, z)}{\int dM \frac{dn}{dM} L_{[\text{CII}]}(M, z)}, \quad (5)$$

with $b(M, z)$ being the halo bias, itself gets diminished to some extent under luminosity scatter, which we explain as follows: The luminosity-weighted average involves the ratio of the luminosity-weighted sum of the halo bias and the sum of the luminosities within a specific halo mass range. Luminosity scatter introduces a relative de-correlation between the luminosity and the halo bias and hence, into the weighted sum. This de-correlated sum is comparatively at a disadvantage to the sum of the luminosities. Therefore, the ratio decreases, and we have a lower luminosity-weighted halo bias. Because of this, the maximum increment in the clustering power spectrum gets somewhat reduced.

Now, this bias diminishing is not specific to this case. We see that the power spectrum at large scales is enhanced by 30 – 40 per cent, although we get ~ 23 per cent increment in the mean intensity when interpreted with the [Leung et al. \(2020\)](#) fit. Therefore, this slight decrement in the luminosity-weighted halo bias is independent of the interpretation of the change in the intensity and the power spectrum. In the argument presented above, we need not assume a specific $L_{[\text{CII}]}$ versus M_{halo} fit (i.e. whether $L_{[\text{CII}]}(M, z)$ represents the fit from mean $L_{[\text{CII}]}$ values, most probable $L_{[\text{CII}]}$ values or any other kind of parametrization) in the no-scatter case. Therefore, unlike the mean intensity, this diminishing in the bias might be unavoidable when we consider the line-luminosity scatter.

5 SUMMARY

In this paper, we show that we can interpret the $[\text{C II}]_{158\mu\text{m}}$ power spectrum with luminosity scatter, where the clustering (large-scale) power spectrum is enhanced, in addition to the shot-noise component. It is valid when we interpret against both the one-to-one $L_{[\text{CII}]}$ versus M_{halo} relation obtained either from mean $L_{[\text{CII}]}$ values or most probable $L_{[\text{CII}]}$ values. In the former case, the enhancement in the power spectrum can be 30 – 40 per cent, whereas it can be up to a factor of ~ 2.9 for the latter. We might note that in cases where scatter is implemented via a semi-analytical approach, to interpret its impact, one might assume a given $L_{[\text{CII}]} - M_{\text{halo}}$ relation such that it is the arithmetic mean of a log-normal scatter with a certain σ (dex). In this case, since $L_{[\text{CII}]}(M, z)$ is defined to be the mean $L_{[\text{CII}]}$ in every halo mass bin, one obtains the mean intensity to be invariant under log-normal scatter. Therefore, one might interpret the impact of luminosity scatter on the shot-noise component with clustering power spectrum not impacted significantly. On the contrary, we derive the line-luminosity scatter from a hydrodynamic and radiative transfer simulation of galaxies, such that the statistical properties (e.g. mean $L_{[\text{CII}]}$, along with mode and σ) vary for every halo mass bin. It is not equivalent to a simple semi-analytical approach, and when we fit a $L_{[\text{CII}]} - M_{\text{halo}}$ relation with mean $L_{[\text{CII}]}$ values, we do not find the mean intensity invariant and interpret the clustering power spectrum to be impacted in this case. We also find that the luminosity-weighted halo bias is slightly diminished, unavoidably,

under luminosity scatter, such that the overall clustering power spectrum is enhanced significantly; this change is comparable to that of the shot-noise component in our case.

The overall slope of the LIM power spectrum would have been modified, at least for the large k -modes, if the shot-noise power spectrum were to dominate in this case. This relative dominance of the individual power spectra components under log-normal scatter depends on how the one-to-one luminosity-halo mass trend might behave, e.g., the slope of the L_{line} versus M_{halo} trend. The slope determines how the halo masses are weighted in luminosity to each other (see [Li et al. 2016](#), sec. 3.2). For a higher slope, the massive halos are weighted more, such that most of the line emission occurs from more over-dense regions, leading to more discretization noise on small scales (see [Kannan et al. 2021](#)).

From the observational perspective of the LIM signal, future experiments might be able to constrain some aspects (e.g. the slope) of the $L_{[\text{CII}]} - \text{SFR}$ and $\text{SFR} - M_{\text{halo}}$ relation ([Karoumpis et al. 2021](#)) from the power spectrum. However, the power spectrum alone might not be able to constrain the scatter information (σ). As we can understand from eq. 4, the same power spectrum can result from different combinations of $L_{[\text{CII}]} - M_{\text{halo}}$ relation (whose amplitude can be parametrized by the log-space average of log-normal scatter or \bar{L}) and σ . Therefore, to better constrain the astrophysics of the LIM signal, one might need to use higher-order statistics, such as the bispectrum.

In summary, we explore frameworks that we can use to interpret the impact of the $[\text{C II}]_{158\mu\text{m}}$ luminosity scatter on the LIM power spectrum. We present an alternative approach where the LIM power spectrum with scatter can be interpreted against the best fit $L_{[\text{CII}]} - M_{\text{halo}}$ relation obtained from the most probable values of $L_{[\text{CII}]}$ distribution. From the perspective of the population distribution of galaxies, the most probable $L_{[\text{CII}]}$ values are a natural choice and conform along the lines of the Bayesian fitting method. Therefore, this alternative approach is a justifiable and robust framework and can be understood in conjunction with the simple model of eq. 4 (as in [Moradinezhad Dizgah et al. 2021](#)) and the slight diminishing of the luminosity-weighted halo bias.

ACKNOWLEDGEMENTS

CSM acknowledges funding from the Council of Scientific and Industrial Research (CSIR) via a CSIR-JRF fellowship, under the grant 09/1022(0080)/2019-EMR-I. KPO is funded by the National Aeronautics and Space Administration (NASA), under award No. 80NSSC19K1651. DN acknowledges the National Science Foundation (NSF) via AST-1909153 and NASA under award No. 80NSSC19K1651. The Cosmic Dawn Center of Excellence is funded by the Danish National Research Foundation under grant No. 140. Part of this research was done using the computing resources available to the Cosmology with Statistical Inference (CSI) research group at IIT Indore.

This research made use of arXiv (<https://arxiv.org>) research-sharing platform, NASA Astrophysics Data System Bibliographic Services and Crossref (<https://www.crossref.org>) citation services. The following softwares have been used: N-body² ([Bharadwaj & Srikant 2004](#)), FoF-Halo-Finder³ ([Mondal et al. 2015](#)), SIMBA⁴ ([Davé et al. 2019](#); [Leung et al. 2020](#)), CLOUDY ([Ferland](#)

² <https://github.com/rajeshmondal18/N-body>

³ <https://github.com/rajeshmondal18/FoF-Halo-finder>

⁴ <http://simba.roe.ac.uk/>

et al. 2013, 2017), `SIGAME`⁵ (Olsen et al. 2015, 2016, 2017; Leung et al. 2020), `NumPy` (Harris et al. 2020), `pandas` (pandas development team 2020; Wes McKinney 2010), `seaborn`⁶ (Waskom 2021), `ProPlot`⁷ (Davis 2021), `WolframAlpha` (<https://www.wolframalpha.com/>), The code used here to compute power spectrum is customized and adapted from N-body (Bharadwaj & Srikant 2004) and ReionYuga⁸ (Choudhury et al. 2009; Majumdar et al. 2014; Mondal et al. 2017)

DATA AVAILABILITY

The simulated data underlying this work will be shared upon reasonable request to the corresponding author(s).

REFERENCES

- Appleby S., Davé R., Kraljic K., Anglés-Alcázar D., Narayanan D., 2020, *MNRAS*, **494**, 6053
- Bharadwaj S., Srikant P. S., 2004, *Journal of Astrophysics and Astronomy*, **25**, 67
- CCAT-Prime collaboration et al., 2021, arXiv e-prints, p. [arXiv:2107.10364](https://arxiv.org/abs/2107.10364)
- Choudhury T. R., Haehnelt M. G., Regan J., 2009, *Monthly Notices of the Royal Astronomical Society*, **394**, 960
- Cothard N. F., et al., 2020, *Journal of Low Temperature Physics*, **199**, 898
- Crites A. T., et al., 2014, in Holland W. S., Zmuidzinas J., eds, *Millimeter, Submillimeter, and Far-Infrared Detectors and Instrumentation for Astronomy VII*. SPIE, doi:10.1117/12.2057207, <https://doi.org/10.1117/12.2057207>
- Davé R., Anglés-Alcázar D., Narayanan D., Li Q., Rafieferantsoa M. H., Appleby S., 2019, *MNRAS*, **486**, 2827
- Davis L. L. B., 2021, *ProPlot*, doi:10.5281/zenodo.5495979, <https://doi.org/10.5281/zenodo.5495979>
- Dumitru S., Kulkarni G., Lagache G., Haehnelt M. G., 2019, *Monthly Notices of the Royal Astronomical Society*, **485**, 3486
- Ferland G. J., et al., 2013, *Rev. Mex. Astron. Astrofis.*, **49**, 137
- Ferland G. J., et al., 2017, *Rev. Mex. Astron. Astrofis.*, **53**, 385
- Fèvre O. L., et al., 2020, *Astronomy & Astrophysics*, **643**, A1
- Gong Y., Cooray A., Silva M. B., Santos M. G., Lubin P., 2011a, *The Astrophysical Journal*, **728**, L46
- Gong Y., Cooray A., Silva M., Santos M. G., Bock J., Bradford C. M., Zemcov M., 2011b, *The Astrophysical Journal*, **745**, 49
- Harris C. R., et al., 2020, *Nature*, **585**, 357
- Hassan S., Davé R., McQuinn M., Somerville R. S., Keating L. C., Anglés-Alcázar D., Villaescusa-Navarro F., Spergel D. N., 2021, arXiv e-prints, p. [arXiv:2109.03840](https://arxiv.org/abs/2109.03840)
- Hopkins P. F., 2015, *MNRAS*, **450**, 53
- Hopkins P. F., 2017, arXiv e-prints, p. [arXiv:1712.01294](https://arxiv.org/abs/1712.01294)
- Ivezić Ž., Connolly A., Vanderplas J., Gray A., 2014, *Statistics, Data Mining and Machine Learning in Astronomy*. Princeton University Press
- Kannan R., Smith A., Garaldi E., Shen X., Vogelsberger M., Pakmor R., Springel V., Hernquist L., 2021, arXiv e-prints, p. [arXiv:2111.02411](https://arxiv.org/abs/2111.02411)
- Karoumpis C., Magnelli B., Romano-Díaz E., Haslbauer M., Bertoldi F., 2021, arXiv e-prints, p. [arXiv:2111.12847](https://arxiv.org/abs/2111.12847)
- Lagache G., 2017, *Proceedings of the International Astronomical Union*, **12**, 228–233
- Leung T. K. D., Olsen K. P., Somerville R. S., Davé R., Greve T. R., Hayward C. C., Narayanan D., Popping G., 2020, *ApJ*, **905**, 102
- Li T. Y., Wechsler R. H., Devaraj K., Church S. E., 2016, *ApJ*, **817**, 169
- Majumdar S., Mellema G., Datta K. K., Jensen H., Choudhury T. R., Bharadwaj S., Friedrich M. M., 2014, *Monthly Notices of the Royal Astronomical Society*, **443**, 2843
- Mondal R., Bharadwaj S., Majumdar S., Bera A., Acharyya A., 2015, *Monthly Notices of the Royal Astronomical Society: Letters*, **449**, L41
- Mondal R., Bharadwaj S., Majumdar S., 2017, *MNRAS*, **464**, 2992
- Moradinezhad Dizgah A., Nikakhtar F., Keating G. K., Castorina E., 2021, arXiv e-prints, p. [arXiv:2111.03717](https://arxiv.org/abs/2111.03717)
- Murmu C. S., Majumdar S., Datta K. K., 2021, *MNRAS*, **507**, 2500
- Olsen K. P., Greve T. R., Narayanan D., Thompson R., Toft S., Brinch C., 2015, *ApJ*, **814**, 76
- Olsen K. P., Greve T. R., Brinch C., Sommer-Larsen J., Rasmussen J., Toft S., Zirm A., 2016, *MNRAS*, **457**, 3306
- Olsen K., Greve T. R., Narayanan D., Thompson R., Davé R., Niebla Rios L., Stawinski S., 2017, *ApJ*, **846**, 105
- Planck Collaboration et al., 2014, *A&A*, **571**, A16
- Robertson B. E., Ellis R. S., Furlanetto S. R., Dunlop J. S., 2015, *ApJ*, **802**, L19
- Schaan E., White M., 2021, *Journal of Cosmology and Astroparticle Physics*, **2021**, 068
- Silva M., Santos M. G., Cooray A., Gong Y., 2015, *The Astrophysical Journal*, **806**, 209
- Sun G., et al., 2021, *ApJ*, **915**, 33
- The CONCERTO Collaboration et al., 2020, *A&A*, **642**, A60
- Thomas N., Davé R., Anglés-Alcázar D., Jarvis M., 2019, *MNRAS*, **487**, 5764
- Vanderplas J., Connolly A., Ivezić Ž., Gray A., 2012, in *Conference on Intelligent Data Understanding (CIDU)*. pp 47 –54, doi:10.1109/CIDU.2012.6382200
- Vieira J., et al., 2020, arXiv e-prints, p. [arXiv:2009.14340](https://arxiv.org/abs/2009.14340)
- Visbal E., Loeb A., 2010, *Journal of Cosmology and Astroparticle Physics*, **2010**, 016
- Waskom M. L., 2021, *seaborn: statistical data visualization*, doi:10.21105/joss.03021, <https://doi.org/10.21105/joss.03021>
- Wes McKinney 2010, in Stéfan van der Walt Jarrod Millman eds, *Proceedings of the 9th Python in Science Conference*. pp 56 – 61, doi:10.25080/Majora-92bf1922-00a
- Wu X., Davé R., Tacchella S., Lotz J., 2020, *MNRAS*, **494**, 5636
- Yang S., Popping G., Somerville R. S., Pullen A. R., Breyse P. C., Maniyar A. S., 2021, arXiv e-prints, p. [arXiv:2108.07716](https://arxiv.org/abs/2108.07716)
- Yue B., Ferrara A., 2019, *Monthly Notices of the Royal Astronomical Society*, **490**, 1928
- pandas development team T., 2020, *pandas-dev/pandas: Pandas*, doi:10.5281/zenodo.3509134, <https://doi.org/10.5281/zenodo.3509134>

This paper has been typeset from a \LaTeX file prepared by the author.

⁵ https://github.com/kpolsen/SIGAME_v2

⁶ <https://seaborn.pydata.org/>

⁷ <https://proplot.readthedocs.io/en/stable/>

⁸ <https://github.com/rajeshmondal18/ReionYuga>